Nonequilibrium phase transitions in systems with infinitely many absorbing states

Iwan Jensen*
Department of Physics and Astronomy, Herbert H. Lehman College, City University of New York, Bronx, New York 10468 and Institute of Physics and Astronomy, University of Aarhus, DK-8000 Aarhus C, Denmark

Ronald Dickman†
Department of Physics and Astronomy, Herbert H. Lehman College, City University of New York, Bronx, New York 10468
(Received 23 February 1993)

We study two nonequilibrium lattice models exhibiting a continuous phase transition from an active state to an absorbing state in which the system is trapped. The models have infinitely many absorbing states. We use one of the models to illustrate how finite-size scaling concepts may be used to enhance computer-simulation studies of the critical behavior. This model is also studied using ordinary steady-state scaling concepts. The results show that the model has the same critical behavior as directed percolation. The applicability of time-dependent simulations, which have proven very efficient in the study of systems with a single absorbing state, is explored extensively using several different initial configurations.

PACS number(s): 05.50.+q, 02.50.−r, 05.70.Ln

I. INTRODUCTION

The study of nonequilibrium many-particle systems is an important problem in many branches of physics, chemistry, biology, and even sociology [1,2]. Some of these systems are known to exhibit kinetic phase transitions; in particular, numerous models have been proposed in order to study the phenomenon of continuous phase transitions. A simple example is the *contact process* (CP) [3–5], which was introduced as a model of an epidemic. In the CP particles annihilate with probability p or else create a new particle at a randomly chosen nearest neighbor provided it is vacant. In addition to the trivial extinct state, the CP has an active steady state (a state in which the population survives indefinitely) for all $d \geq 1$ when $p \leq p_c(d)$ [4,5]. The CP may be seen as a lattice version of Schlögl's first model [6–8], which is defined in terms of the reaction scheme $X \rightleftharpoons 2X$, $X \rightleftharpoons 0$. If we discard the spontaneous creation process, $0 \rightarrow X$, we are left with an autocatalytic chemical reaction whose lattice version obviously is closely related to the CP. In computer simulations of the CP one usually uses sequential updating. If we use simultaneous updating, we arrive at a cellular automaton [9–11]. As a cellular automaton, the contact process is closely related to *dynamical* directed percolation (DP) [12–15]. It has been shown that Schlögl's first model [16,17] and directed percolation [13] are equivalent to Reggeon field theory (RFT) [18–22]. So far we have considered only one-component models. In recent years multicomponent models have attracted a great deal of attention. The best known example is probably the monomer-dimer model of Ziff, Gulari, and Barshad (ZGB) [23–26]. This model was proposed in order to study the oxidation of carbon monoxide on a catalytic surface. The ZGB model exhibits a second-order phase transition from an oxygen-covered state to an active state and a first-order transition to a CO-covered state.

One of the major achievements in the study of nonequilibrium phase transitions is the discovery that all of the models mentioned above belong to the same universality class. The study of many other models [27–38] demonstrates the robustness of DP critical behavior in spite of quite dramatic differences in the evolution rules of the various models. Presently there is substantial evidence in favor of the hypothesis that models with a scalar order parameter exhibiting a continuous transition to a *unique* absorbing state generically belong to the universality class of directed percolation. This DP conjecture was first put forward by Grassberger [8] and Janssen [7] and later extended by Grinstein, Lai, and Browne [25] to multicomponent models.

The universality of DP critical behavior for models with a unique absorbing state is well established, but the study of models with more than one absorbing state is still in its infancy. That models with more than one absorbing state can exhibit new critical behavior was first demonstrated by Grassberger, Krause, and von der Twer [39] in a study of a model involving the processes $X \rightarrow 3X$ and $2X \rightarrow 0$. This model is very similar to a class of models known as branching annihilating walks (BAW's) [36]. In the BAW a particle jumps, with probability p, to a nearest neighbor, and if this site is occupied both particles annihilate. With probability $1-p$ the particle produces n offspring which are placed on the neighboring sites. If an offspring is created on a site which is already occupied, it annihilates with the occupying particle leaving an empty site. For n even these models have non-DP behavior [37], while for n odd the behavior is compatible with DP [38]. Note that in both the model proposed by Grassberger, Krause, and von der Twer and in BAW's with an even number of offspring the number of particles is conserved modulo 2. This conservation law might be responsible for the non-DP behavior.

At present there are no clear ideas about the possible universality classes for models with more than one ab-

sorbing state; e.g., do a wide variety of models exhibit a similar, though possibly non-DP, critical behavior, or does each model have its own? In this paper we study models with infinitely many absorbing states, or, to be more precise, models in which the number of absorbing states grows exponentially with system size. Earlier studies of dimer-trimer [40] and dimer-dimer [41] reactions suggested that such models might have non-DP critical behavior. These results were, however, cast into doubt by a study of the pair contact process (PCP) [42], which yielded DP critical exponents for a one-dimensional model with infinitely many absorbing states. In this paper we report further results for the pair contact process and results for a new model, the dimer reaction model. The one-dimensional versions of both models belong to the DP universality class.

The remainder of this paper is organized as follows. In Sec. II we introduce the models and the phenomenology concerning their critical behavior. In Sec. III we report results from computer simulations of the PCP and describe important concepts and various computer-simulation methods pertinent to the study of continuous phase transitions. Section III A covers steady-state scaling and Sec. III B contains a thorough description of finite-size scaling concepts. Time-dependent simulations have proven very efficient in the study of models with a unique absorbing state. The applicability of this method to models with infinitely many absorbing states is studied in Sec. III C. Our results on the dimer reaction model are reported in Sec. IV.

II. MODELS WITH INFINITELY MANY ABSORBING STATES

The systems considered in this paper are nonequilibrium lattice models or *interacting particle systems* [4,5] evolving according to a Markov process with local, intrinsically irreversible transition rules. The models typically involve spontaneous annihilation of particle clusters with probability p, independent of the states of sites outside the cluster; autocatalytic creation of particles with a probability depending on the number of occupied sites in some neighborhood of the vacancy; and diffusion of particles. When both creation and annihilation are contingent on the presence of clusters of two or more particles, the evolution may terminate in one of many absorbing configurations. In addition to these trivial states the systems may possess (in the infinite-size limit) a nontrivial ("active") steady state when p is sufficiently small. The region of the phase diagram in which there is an active steady state is called the supercritical region, as opposed to the subcritical region, in which the absorbing states are the only steady states. The models studied in this paper exhibit a continuous phase transition from the active to the absorbing states at some critical value p_c. The order parameter $\bar{\rho}$ decays asymptotically as $\bar{\rho} \propto (p_c - p)^{\beta}$ when $p \to p_c -$. Figure 1 illustrates the general ideas mentioned above by showing the "phase diagram" for the pair contact process, which will be defined below.

The pair contact process is a simple one-component model in which nearest-neighbor pairs of particles annihilate each other (with probability p) or else create (with probability $1-p$) a particle at a randomly chosen nearest neighbor provided it is vacant. Since the creation of a particle next to a pair creates at least one additional pair, the evolution rules for pairs are very similar to those for particles in the CP. The absorbing state is now one without pairs and in this sense it is unique, but there are many such states from the particle point of view. The number of absorbing states is $>2^{N/2}$ on a one-dimensional (1D) lattice of N sites. The evolution rules for pairs suggest that this model should exhibit the same critical behavior as the contact process, assuming that the concentration of pairs is the appropriate order parameter. However, the existence of infinitely many absorbing states on the particle level could lead to a new critical behavior. Steady-state simulations of the one-dimensional version, including a thorough finite-size scaling analysis, presented in Secs. III A and III B, are, however, consistent with the same critical behavior as the contact process.

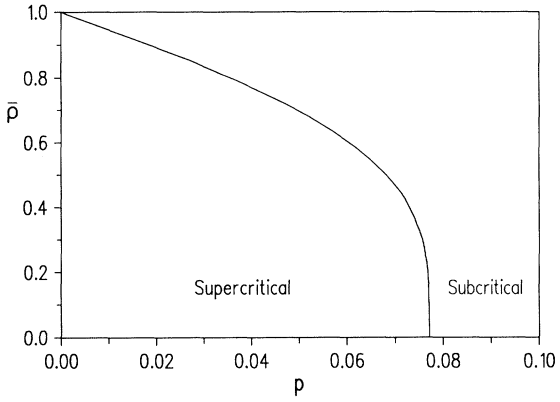

FIG. 1. The steady-state concentration of pairs in the pair contact process as a function of the pair annihilation probability. For $p < p_c \simeq 0.0771$ the system is in the supercritical region and has an active steady state. At p_c the model exhibits a continuous phase transition to the absorbing state. The region $p > p_c$ is called the subcritical region and here the absorbing state is the only steady state.

We have studied another model which exhibits a continuous phase transition from an active steady state to one of a multitude of absorbing configurations. The *dimer reaction model* (DR) is based on a simpler model introduced by Browne and Kleban (BK) [30]. In the BK model particles rain down on a lattice at some constant rate, and adsorb (at least temporarily) at vacant sites. Suppose a particle has just adsorbed at site i. If all of the neighbors of i are vacant, the particle remains at i, but if one or more of the neighbors is occupied, the particle remains only with probability p. With probability $1-p$ there is a reaction between the new arrival and one of the neighboring particles (chosen at random, if there is a choice), which removes these two particles from the lattice. For small p the process attains an active steady state, but as $p \to p_c$ there is a continuous transition to the absorbing state with all sites filled. For the one-dimensional BK model, $p_c = 0.2765(5)$. The transition

belongs to the directed percolation class [31].

In the DR (on a one-dimensional lattice) particles may not occupy neighboring sites. if sites i, $i-1$, and $i+1$ are vacant, we say that site i is *open*; adsorption happens only at open sites. If we think of the sites as corresponding to *bonds* in the *dual* lattice, the particles correspond to dimers occupying bonds in the dual lattice. Suppose a particle has just arrived at site i. If sites $i-3$, $i-2$, $i+2$, and $i+3$ are all vacant, the particle remains. If any of the four sites is occupied, the new particle reacts with one other particle with probability $1-p$ and remains with probability p. The second neighbors have priority in the reaction: the new particle can react with a third neighbor only if both second-neighbor sites are empty. The reaction rules are illustrated in Fig. 2. We note that reactions with third neighbors are essential, for without them there is no active steady state even for $p=0$. We do not believe second-neighbor priority to be essential for the existence of an active steady state.

There are many absorbing states for the DR: any configuration without a three-site vacancy cluster, i.e., devoid of open sites. Of these absorbing states, the one with maximal particle density consists of alternating vacant and occupied sites; in the one with minimal density, occupied sites alternate with pairs of vacant sites. Clearly any sequence . . . *OGOGOGO* . . . , where *O* means occupied and *G* is a one- or two-site gap, is absorbing. The obvious choice for the order parameter is the density of open sites ρ_o. For $p=0$ simulations yield $\rho_o \simeq 0.6$; they show ρ_o decreasing continuously to zero as p approaches $p_c \simeq 0.2640$. At the same time ρ_p, the particle density, increases from zero to about 0.418(1) at the transition. For $p=1$ (no reactions) the DR becomes dimer random sequential adsorption, for which $\rho_p=(1-e^{-2})/2 = 0.43233\ldots$ [43,44]. We studied the DR in three kinds of simulations, which focused on (1) the mean poisoning time, starting from an empty lattice, (2) the steady-state behavior of the open site and particle densities, and (3) the survival probability, number of open sites, and spreading of open sites, starting from a configuration with a single open site.

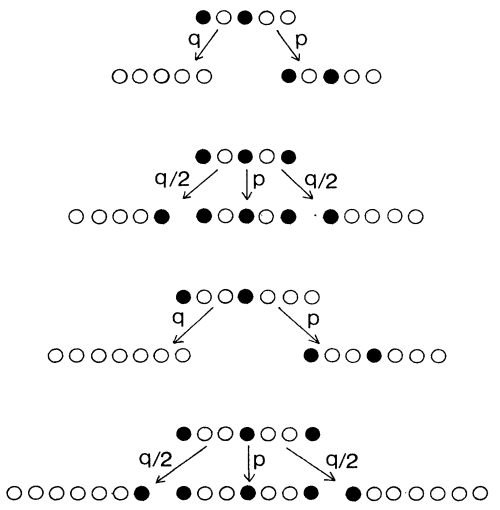

FIG. 2. Dimer reaction rules involving a newly adsorbed particle (at the center of the cluster) and a second or third neighbor. The total reaction probability (given a neighbor) is $q=1-p$. Reaction probabilities (i.e., for the first and third processes) are symmetric under reflection.

Models with infinitely many absorbing states arise naturally in the study of reactions catalyzed by a surface as soon as the absorption mechanism for the various species (normally two) require more than one vacant site. Two such models, the dimer-trimer model [40] and the dimer-dimer model [41], have been introduced recently.

The dimer-trimer model is a variation of the ZGB model. Dimers A_2 may adsorb onto a nearest-neighbor pair of vacancies and subsequently dissociate. Likewise, a trimer B_3 may undergo dissociative adsorption onto three nearest-neighbor vacancies. A and B nearest-neighbor pairs react instantly and the product AB desorbs. A_2 adsorption is attempted with probability p and B_3 adsorption with probability $1-p$, thus making p the only control parameter. Computer simulations [40] on triangular lattices showed that this model has a phase diagram with a trimer saturated state for $p<p_1$, a dimer saturated state for $p>p_2$, and an active steady state for intermediate values. A saturated state is a configuration where only isolated empty sites are left. Such a state is obviously an absorbing state for the process, and one immediately notices that the number of such states grows exponentially with system size. The transition at $p_1=0.3403(2)$ is continuous, whereas the transition at $p_2=0.4610(8)$ is discontinuous. Critical exponents β_A and β_B describing, respectively, the behavior of the concentrations of A and B near p_1 may be defined as $\rho_A \propto (p-p_1)^{\beta_A}$ and $\rho_B^{\rm sat}-\rho_B \propto (p-p_1)^{\beta_B}$, where $\rho_B^{\rm sat}$ is the saturation concentration of B at p_1. Steady-state computer simulations [40] yielded $\beta_A=0.80(6)$ and $\beta_B=0.63(5)$. While the estimate for β_A is well above the DP value 0.57, the estimate for β_B could be consistent with DP behavior. The dimer-trimer model was also studied using time-dependent simulations (see Sec. III C for a description of this method). As there is no unique absorbing state in this model, one has to make a choice of initial configuration. ben-Avraham and Köhler chose to start each run on a different random configuration, an absorbing state except for a triplet of vacancies at the center. They estimated that $\delta=0.40\pm0.01$, $\eta=0.28\pm0.01$, and $z=1.19\pm0.01$. These exponent estimates clearly differ from the DP values [15], $\delta=0.460\pm0.006$, $\eta=0.214\pm0.008$, and $z=1.134\pm0.004$, suggesting that the dimer-trimer model belongs to a new universality class. Note, however, that the exponents do not satisfy the hyperscaling relation $dz=4\delta+2\eta$ [17]. This could signal that the numerical values had not yet converged to their asymptotic values or that the error bars are not conservative enough.

The dimer-dimer (DD) model for the oxidation of hydrogen on a metal surface is based on the Langmuir-Hinshelwood mechanism (both reactants are adsorbed on the surface). The model was studied in two versions. In the first model, DD1, O_2 adsorption is attempted with probability p and H_2 adsorption with probability $1-p$. Both O_2 and H_2 require a nearest-neighbor pair of vacan-

cies and will dissociate upon adsorption. Nearest-neighbor H and O react to form OH residing on a single site. OH will react with H (OH) forming H_2O (leaving behind one O) which desorbs immediately. In addition, H is allowed to diffuse on the surface. The second model, DD2, is like DD1 except that if H_2 is adsorbed but does not react it will recombine and leave the surface at once. The DD1 model exhibits two continuous phase transitions. When $p<p_1$, the steady state is an absorbing state with a mixture of adsorbed O and OH, and isolated single vacancies. When $p>p_2$ the lattice becomes completely covered with H, which is thus a unique absorbing state. For $p_1<p<p_2$ there is an active steady state with an ongoing production of H_2O. Computer simulations of the DD1 model in the vicinity of p_1 yielded estimates for the critical exponents describing the behavior of the concentration of adsorbed particles in this region: $\rho_H \propto (p-p_1)^{\beta_H^l}$ and $\rho_{O+OH}^{sat}-\rho_O-\rho_{OH} \propto (p-p_1)^{\beta_O^l}$, where $\rho_{O+OH}^{sat} \simeq 0.907$ is the saturation value of O and OH coverage. Albano [41] estimates that $\beta_H^l=\beta_O^l \sim \frac{1}{2}$ with an uncertainty of approximately 5–10 %. The similar exponents describing how ρ_O, ρ_{OH}, and $1-\rho_H$ vanish at p_2 were found to be 2, again with an estimated uncertainty of 5–10 %. The former result may be seen as an indication of a new universality class, though the results could be marginally consistent with DP behavior, $\beta \simeq 0.57$. The latter result is very surprising, as the transition at p_2 is into a unique absorbing state. As the DD2 model includes recombination and desorption of H_2, this model has only one phase transition at $p_1^{(2)}$ from an active state to an absorbing state containing O, OH, and isolated vacancies. For this model it was found [41] that $\beta_H^{(2)} \simeq \frac{2}{3}$ and $\beta_O^{(2)} \simeq \frac{1}{2}$, again with an uncertainty of about 5–10 %. These results are again marginally consistent with directed percolation. In view of the difficulty in establishing the critical behavior of the dimer-dimer and dimer-trimer models, we decided to perform extensive studies of the PCP and the DR, which present infinitely many absorbing states in the simpler context of single-component, one-dimensional models.

III. RESULTS FOR THE PAIR CONTACT PROCESS

In this section we report the results of extensive computer simulations of the pair contact process. We demonstrate how steady-state and finite-size scaling concepts may be used to study nonequilibrium models with infinitely many absorbing states. The results place the PCP firmly in the DP universality class. Finally, we examine the applicability of time-dependent simulations to models without a unique absorbing state. Our results show that estimates for the critical exponents depend crucially on the way in which we prepare the initial configuration. As shown in Sec. III C, we obtain DP exponents only when using system-generated critical absorbing states as initial configurations.

A. Steady-state behavior

In this section we discuss the static critical behavior of the models introduced above. Critical points are characterized by power-law divergencies of the correlation length and the relaxation time. Consequently, in order to obtain reliable results close to the critical point, one has to study large systems over long times, which means a heavy demand of CPU time. One normally starts the system far from any absorbing state, e.g., in the case of the PCP, with all sites occupied. Starting from this state, one lets the system evolve until, after a relaxation time τ, the steady state is obtained. Once in the steady state, one makes data measurements at various time intervals up to some preset maximal time and performs a time average. Figure 3 shows a typical time evolution for the concentration of pairs in the PCP. An ensemble average is obtained by averaging the results from several independent samples. In the absence of evidence to the contrary, one assumes that the ensemble average equals the time average.

1. Critical behavior

If we assume that the critical behavior is described by generalized homogeneous functions, a simple consequence is that quantities such as the order parameter, the susceptibility, etc., have power-law dependence close to the critical point [45]. In particular, we find that the order parameter $\bar{\rho}$ (where the bar will be used to indicate the steady-state value) decays as

$$\bar{\rho} \propto |p_c-p|^{\beta} \tag{1}$$

in the supercritical regime, where β is the order parameter critical exponent. Likewise, we expect that the "susceptibility" $\bar{\chi}$ per site behaves as

$$\bar{\chi}=L^d(\langle \rho^2 \rangle - \langle \rho \rangle^2) \propto |p_c-p|^{-\gamma} , \tag{2}$$

where L is the linear extension of the system. We call $\bar{\chi}$ the susceptibility because it is a quantity analogous to the susceptibility as defined for equilibrium magnetic systems. Actually, $\bar{\chi}$ is just a measure of the typical size of fluctuations. The divergence of the susceptibility shows that fluctuations become dominant as one approaches the critical point. In Fig. 4 we have plotted $\bar{\rho}$ and $\bar{\chi}$ in the PCP as a function of the distance from the critical point

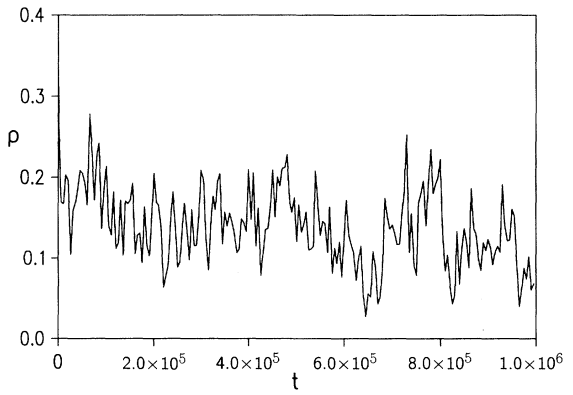

FIG. 3. Typical time evolution for the concentration of pairs of the pair contact process for system size $L=4096$ at $p=0.0771$.

$p_c - p$ on a log-log scale, where we used $p_c = 0.0771$. We will justify our choice for p_c in the next section. The results for $\bar{\rho}$ and $\bar{\chi}$ were obtained by averaging over typically 100 independent samples. The number of time steps and system sizes varied from $t = 5000$, $L = 512$ far from p_c to $t = 500\,000$, $L = 8192$ closest to p_c. One clearly sees that the power-law behavior is confirmed, although the results for $\bar{\chi}$ are somewhat messy. From these results we estimate that $\beta = 0.28(1)$ and $\gamma = 0.53(5)$, where the figure in parentheses indicates the estimated uncertainty on the last digit. These results are in good agreement with the typical estimates for directed percolation in (1+1) dimensions $\beta = 0.2769(2)$ [46] and $\gamma = 0.544(1)$ [47,48].

Note that Eqs. (1) and (2) hold true only in the limit of infinite system size. As in equilibrium second-order phase transitions we assume that the (infinite-size) nonequilibrium system features a length scale which diverges at criticality as

$$\xi(p) \propto |p_c - p|^{-\nu_\perp} , \tag{3}$$

where $\nu_\perp$ is the correlation length exponent in the space direction. Any measurable quantity will depend strongly on system size once the correlation length becomes comparable to the linear extension L of the system. A further complication in steady-state simulations is the divergence of the relaxation time near the critical point. Letting t_R denote some characteristic time scale, e.g., the time it takes to reach the steady state, we assume that when p_c is approached from the subcritical region

$$t_R(p) \propto |p_c - p|^{-\nu_\parallel} , \tag{4}$$

where $\nu_\parallel$ is the correlation length exponent in the time direction. Thus a typical time signal from a system near criticality will exhibit large fluctuations with long lifetimes, as seen in Fig. 3.

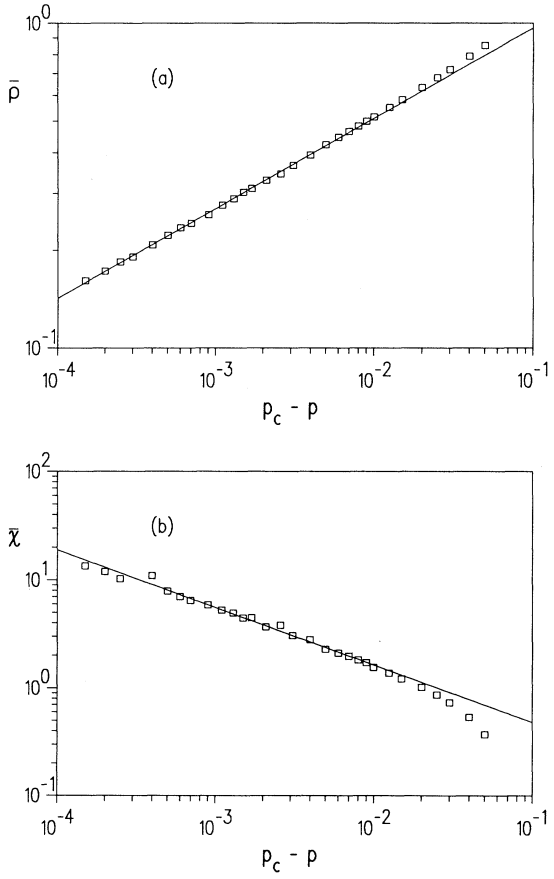

FIG. 4. Panel (a) shows a low-log plot of the steady-state concentration of pairs $\bar{\rho}$ vs the distance from the critical point with $p_c = 0.0771$. The slope of the line is $\beta = 0.277$. Panel (b) shows a log-log plot of the steady-state susceptibility $\bar{\chi}$ vs the distance from the critical point with $p_c = 0.0771$. The slope of the line is $\gamma = 0.53$.

B. Finite-size scaling

The applicability of steady-state computer simulations has been greatly enhanced by finite-size scaling methods. The idea of finite-size scaling was pioneered by Fisher and co-workers in the early 1970s [49,50]. Here we will follow the work of Aukrust, Browne, and Webman [31] and show how finite-size scaling of static and dynamic quantities may be used to determine p_c various critical exponents.

From the nature of the models studied, it is clear that when the system is small it will enter the absorbing state fairly quickly, even for values of p in the supercritical region. In Fig. 5(a) we show the concentration of pairs as a function of time at $p = 0.0771$ for a system of size $L = 128$. $\rho(t)$ almost immediately reaches a reasonably steady value somewhat obscured by large fluctuations. After the system has reached this quasisteady state, it can spend a long time there before it finally enters the absorbing state. Figure 5(b) shows $\rho_s(p,L,t) = \langle \rho(p,L,t,s) \rangle_s$ versus t for various values of L at $p = 0.0771$. $\rho(p,L,t,s)$ is the coverage fraction for a particular sample s; the subscript s will be used to indicate that the average is taken over the *surviving* samples, i.e., the average includes only those samples which have not yet entered an absorbing state. The number of initial samples varied from 2000 for $L = 128$ to 250 for $L = 2048$; in all cases at least 200 samples survived to the end of the simulations. Figures 5(a) and 5(b) show that in spite of a strong tendency to enter the absorbing state, ρ_s does attain a well-defined value and we can thus study $\rho_s(p,L)$ as a function of p and L in the critical region.

1. Static behavior

We expect finite-size effects to become important when the correlation length $\xi(p) \propto |p - p_c|^{-\nu_\perp} \sim L$, so that the basic length is the scaled length $L/\xi(p) \sim L|p - p_c|^{\nu_\perp}$. The ansatz underlying finite-size scaling is that the various quantities depend on system size through the ratio $L/\xi(p)$, or equivalently through the variable $|p_c - p| L^{1/\nu_\perp}$. Thus we assume that the order parameter depends on system size and distance from the critical point as

$$\rho_s(p,L) \propto L^{-\beta/\nu_\perp} f((p - p_c) L^{1/\nu_\perp}) , \tag{5}$$

such that at p_c

$$\rho_s(p_c,L) \propto L^{-\beta/\nu_\perp} \tag{6}$$

and

$$f(x) \propto x^{\beta} \text{ for } x \to \infty , \tag{7}$$

so that Eq. (1) is recovered when $L \to \infty$ in the critical region. For values of p in the supercritical regime ρ_s should be independent of L for $L \gg \xi(p)$. In the subcritical regime one expects ρ_s to decay faster than a power law. Thus p_c may be determined as the value of p yielding a straight line in a log-log plot of ρ_s versus L.

For the susceptibility we expect

$$\chi_s(p,L) \propto L^{\gamma/\nu_\perp} g((p-p_c)L^{1/\nu_\perp}) \tag{8}$$

and

$$\chi_s(p_c,L) \propto L^{\gamma/\nu_\perp} . \tag{9}$$

Figure 6(a) shows the average concentration of pairs $\rho_s(p,L)$ in the quasisteady state as a function of L on a log-log scale for various values of p in the critical region. From this we clearly see that $p=0.0771$ is compatible with a power-law behavior, whereas $p=0.0770$ is supercritical and $p=0.0772$ is subcritical, leading to the estimate $p_c=0.0771(1)$. Figure 6(b) shows a log-log plot of the susceptibility $\chi_s(p_c,L)$ as a function of L. The number of time steps t and independent samples N varied from $t=1000$, $N=25\,000$ for $L=16$ to $t=500\,000$, $N=100$ for $L=8192$. From the slopes of the critical curves we estimate that $\beta/\nu_\perp=0.255(5)$, which when combined with the standard DP value $\beta=0.277(1)$ yields $\nu_\perp=1.09(3)$ and $\gamma/\nu_\perp=0.50(1)$ and thus $\gamma=0.55(4)$, in good agreement with the direct estimate given above. The estimate for $\nu_\perp$ is also in excellent agreement with the more precise estimate $\nu_\perp=1.0972(6)$ obtained from transfer-matrix methods [47]. From the graphs in Fig. 6 we see that the slope for small L already reflects the relevant exponent ratio $\beta/\nu_\perp$ or $\gamma/\nu_\perp$, while the off-critical evolutions veer off the simple power law for large L. Thus finite-size scaling analysis can yield reliable information on exponents using even small system sizes ($L \leq 200$). Large-L studies are needed to fix the critical point with precision.

In the quasisteady state one may also study the probability distribution function $P_L(\rho_s)$ for $\rho_s(p_c,L)$ as one varies the system size L. In the critical region one can

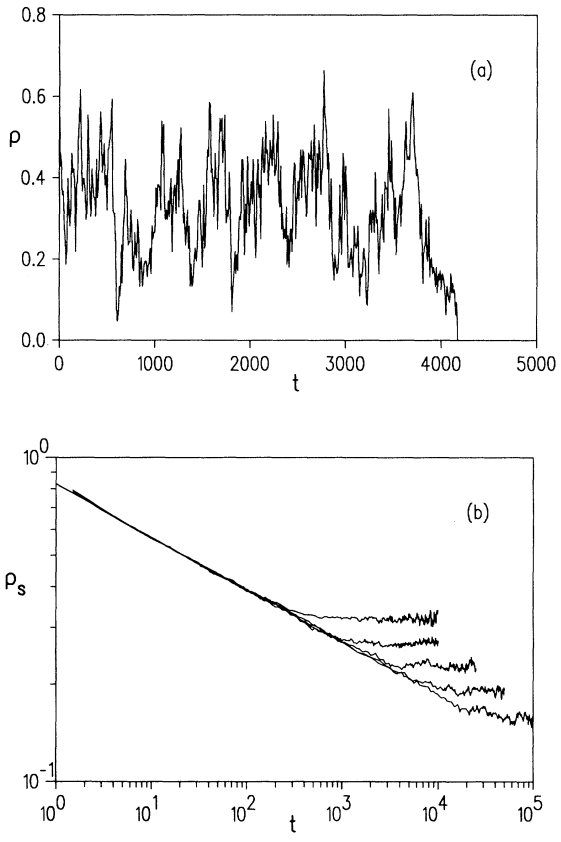

FIG. 5. Panel (a) shows the time evolution of the concentration of pairs for $L=128$ and $p=0.0771$. Panel (b) shows the average number of pairs in the surviving samples, $\langle \rho(p,L,t) \rangle$, as a function of time at $p=0.0771$, with from top to bottom $L=128$, 256, 512, 1024, and 2048.

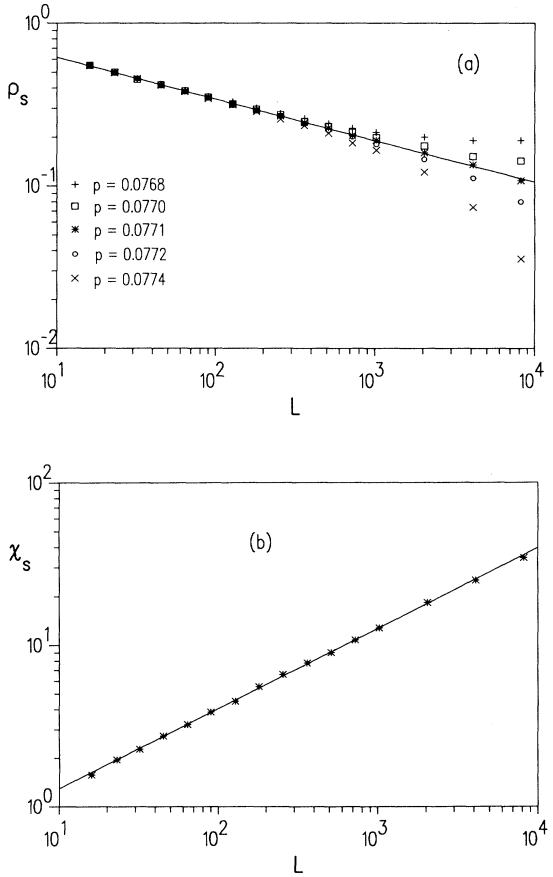

FIG. 6. (a) $\rho_s(p,L)$ vs L for various values of p and (b) $\chi_s(p_c,L)$ vs L. The slopes of the lines are (a) $\beta/\nu_\perp=0.254$ and (b) $\gamma/\nu_\perp=0.50$.

express the distribution function in terms of a scaling function $\tilde{P}$ as [31,51]

$$P_L(\rho_s)=L^{\beta/\nu_\perp}\tilde{P}(\rho_s L^{\beta/\nu_\perp},\xi/L) . \quad (10)$$

In Fig. 7(a) we plot $P_L(\rho_s)L^{-\beta/\nu_\perp}$ versus $\rho_s L^{\beta/\nu_\perp}$, and as one would expect from Eq. (10) we see the data collapse onto a single curve. The inset shows the unscaled data. A consequence of this scaling collapse is of course that the position of the maximum of the probability distribution function scales as $X_{\max}(L)\propto L^{-\beta/\nu_\perp}$, and the value at the maximum scales as $Y_{\max}(L)\propto L^{\beta/\nu_\perp}$. Figure 7(b), which shows $X_{\max}$ and $Y_{\max}$ as functions of L, clearly demonstrates this fact. Once we have the probability distribution we can calculate the various moments $\langle\rho^k\rangle=\int_0^1\rho^k P_L(\rho)d\rho$. In Fig. 7(c) we show a log-log plot of $\langle\rho\rangle$ and $\chi=L(\langle\rho^2\rangle-\langle\rho\rangle^2)$ as a function of the system size L. From Eq. (10) it follows that $\langle\rho\rangle\propto L^{-\beta/\nu_\perp}$, where we naturally recover the earlier result of Eq. (6), and $\langle\rho^2\rangle\propto L^{-2\beta/\nu_\perp}$, from which we get that $\chi=L^d(\langle\rho^2\rangle-\langle\rho\rangle^2)\propto L^{(d\nu_\perp-2\beta)/\nu_\perp}$. If we compare this with the earlier result, Eq. (9), we see that the exponents β, $\nu_\perp$, and γ must obey the hyperscaling relation

$$\gamma=d\nu_\perp-2\beta . \quad (11)$$

In Fig. 7(c) the expected power-law behavior is clearly seen, and the slopes of the lines yield the estimates $\beta/\nu_\perp=0.255(5)$ and $\gamma/\nu_\perp=0.50(1)$, in full agreement with earlier estimates.

2. *Dynamical behavior*

So far we have concerned ourselves mainly with the static scaling behavior; now we turn our attention to the dynamical behavior, i.e., the scaling properties of time-dependent quantities. There are several ways of defining a characteristic time τ for the system under investigation. Aukrust, Browne, and Webman chose to measure the average time for a system to enter the absorbing state, defined as the sample average of the quantity

$$\tau_s=\sum_t t\rho(p,L,t,s)\Big/\sum_t \rho(p,L,t,s) . \quad (12)$$

We can see that τ_s is a measure of a characteristic time for a particular sample to cover by taking the example of a pure exponential relaxation for $\rho(t)$, where if $\rho(t)\propto\exp(-t/\alpha)$, then $\tau_s\sim\alpha$.

One may also define τ as the time it takes to $\rho(L,t)$ to reach the quasisteady state. In this study we have chosen to define $\tau(p,L)$ as the time it takes for half the sample to enter an absorbing state. For values of p deep in the subcritical region or for small system sizes, $\tau(p,L)$ is naturally small. Equation (4) leads to the finite-size scaling form

$$\tau(p,L)\propto L^y h((p-p_c)L^{1/\nu_\perp}) , \quad (13)$$

where $y=\nu_\parallel/\nu_\perp$ is the usual dynamical exponent, similar to the one defined in equilibrium cases [52]. At p_c we thus have

$$\tau(p_c,L)\propto L^y . \quad (14)$$

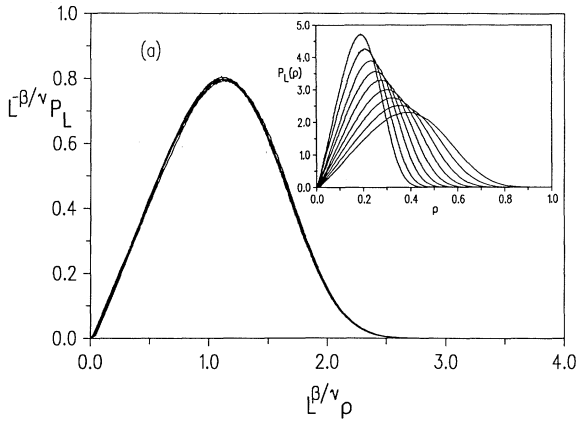

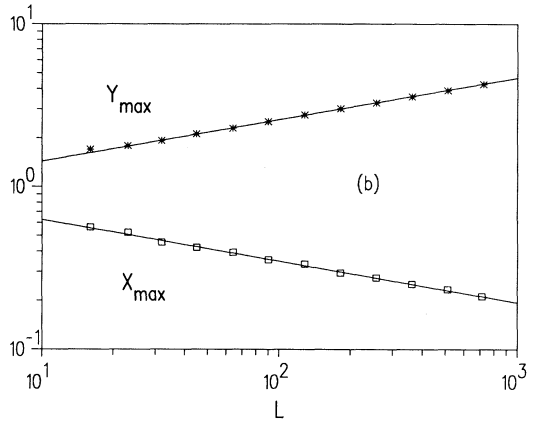

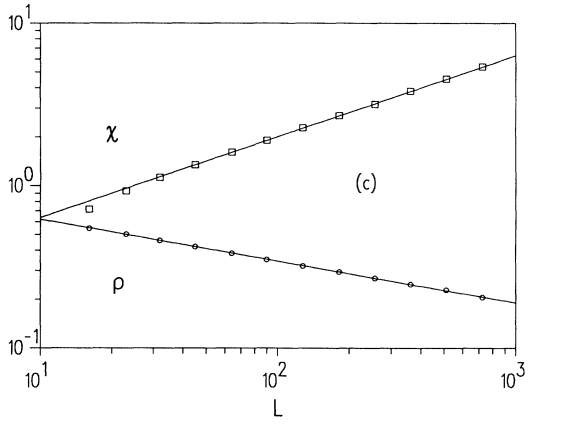

FIG. 7. Panel (a): $P_L L^{-\beta/\nu_\perp}$ vs $L^{\beta/\nu_\perp}$ for $p=0.0771$ for various system sizes L with $\beta/\nu_\perp=0.255$. The inset shows the unscaled data. Panel (b): The maximum $Y_{\max}$ of P_L, and its position $X_{\max}$ vs L on a log-log scale. The slopes of the lines are $\beta/\nu_\perp=0.255$ from $Y_{\max}$ and $-\beta/\nu_\perp=-0.255$ from $X_{\max}$. Panel (c): Log-log plot of $\langle\rho\rangle$ and $\chi=L(\langle\rho^2\rangle-\langle\rho\rangle^2)$ vs L, where the averages are obtained as the first and second moments of the probability distribution $P_L(\rho)$ at p_c. The slopes of the lines are $-\beta/\nu_\perp=-0.255$ from ρ and $\gamma/\nu_\perp=0.50$ from χ.

In the supercritical regime any finite system will eventually enter the absorbing state. However, one expects that $\tau(p,L)$ will grow faster than a power law in L. Figure 8 shows $\tau(p,L)$ as a function of L for values of p in the critical region. Again we see the off-critical curves veering away from a power-law behavior, confirming that $p_c=0.0771$. The slope of the curve for p_c leads to the estimate $y=1.59(3)$. Using the $(1+1)$-d directed percolation values [47] $\nu_\parallel=1.733(1)$ and $\nu_\perp=1.0972(6)$, we have $y=\nu_\parallel/\nu_\perp=1.579(2)$, which is in excellent agreement with our estimate.

One may also study the dynamical behavior by looking at the time dependence of the mean fraction $\rho(p_c,L,t)$ of pairs at p_c. Note that this quantity is different from ρ_s because we now take the average over all samples, including the ones that have entered the absorbing state. For $t\gg1$ and $L\gg1$ one can assume a scaling form

$$\rho(p_c,L,t)\propto L^{-\beta/\nu_\perp} f(t/L^y)\ . \tag{15}$$

In Fig. 9 we have plotted $\rho(p_c,L,t)L^{\beta/\nu_\perp}$ as a function of t/L^y, with the inset of that figure showing the unscaled data. As can be seen, one can obtain a very good data collapse, confirming the validity of the scaling assumption. At p_c the system shows a power-law behavior for $t<L^y$ before finite-size effects become important. Thus for $L\gg1$ and $t<L^y$ we have that $\rho(p_c,L,t)\propto t^{-\theta}$. From Eq. (15) we see that this is the case for large L only if the scaling relation

$$\theta=\beta/(\nu_\perp y)=\beta/\nu_\parallel \tag{16}$$

holds. Using the unscaled data in Fig. 9 we obtain, from the short-time behavior, the estimate $\theta=0.160(5)$. This is in excellent agreement with directed percolation, for which the earlier cited estimates yields $\theta=\beta/\nu_\parallel=0.1598(3)$.

C. Time-dependent behavior

In this section we will discuss another way of studying models with absorbing states. This method, pioneered by Grassberger and de la Torre [17], utilizes the fact that the model has absorbing states by studying the evolution of an ensemble of systems, each of which starts close to a "typical" absorbing state. One can then ask questions such as, What is the probability that particles are still present at time t, and how many particles are there on the average? In the case of the ordinary contact process one would choose to start all systems with just one particle at the center of the lattice. However, in the case of models with infinitely many absorbing states we are faced with a problem, because it is not clear which initial configuration to use. As will become evident in the following, the estimates for the critical exponents depend strongly on the choice of initial configuration (the estimates for p_c are far less sensitive).

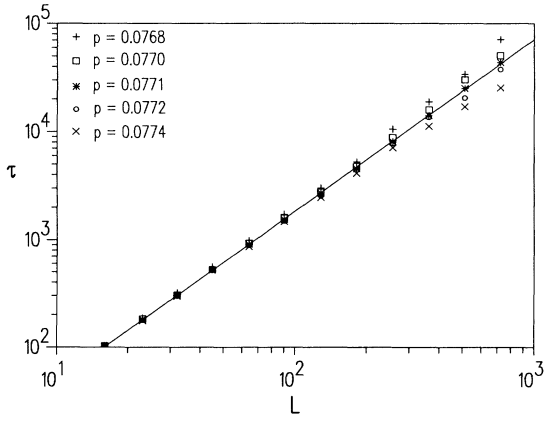

FIG. 8. $\tau(p,L)$ vs L for various values of p in the critical region. The slope of the line yields the value $y=\nu_\perp/\nu_\parallel=1.59$.

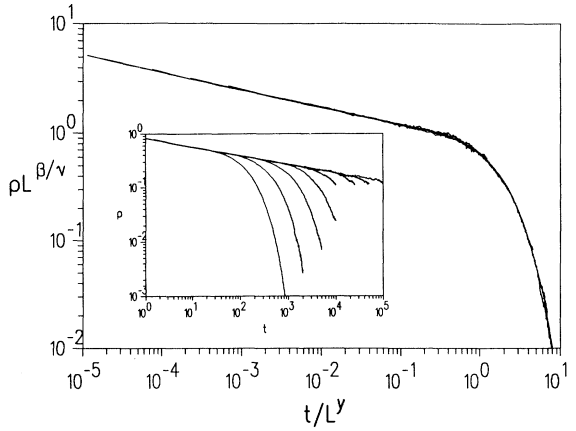

FIG. 9. $\rho(p_c,L,t)L^{\beta/\nu_\perp}$ vs t/L^y with $\beta/\nu_\perp=0.254$ and $y=1.59$ for various values of L. The inset shows the unscaled data, with from left to right, $L=16, 32, \ldots, 2048$.

1. Scaling ansatz

According to the scaling hypothesis [17], one expects that any function of x, t, and Δ (where $\Delta=p_c-p$) depends on these variables only through x^2/t^z and $\Delta t^{1/\nu_\parallel}$, times some power of x^2, t, or Δ. As before, $\nu_\parallel$ is the correlation length exponent in the time direction and z is *not* the dynamic exponent of equilibrium critical phenomena. For the particle density one expects

$$\rho(x,t)\propto t^{\eta-dz/2}F(x^2/t^z,\Delta t^{1/\nu_\parallel})\ , \tag{17}$$

and for the probability of survival, i.e., the probability that the system has not entered the absorbing state at time t, one expects

$$P(t)\propto t^{-\delta}\phi(\Delta t^{1/\nu_\parallel})\ , \tag{18}$$

where η and δ are further critical exponents, while F and ϕ are universal scaling functions.

From Eq. (17) one finds for the mean number of particles $\bar{n}(t)$ and the mean-square distance of spreading $\bar{R}^2(t)$

$$\bar{n}(t)=\int d^dx\,\rho(x,t)\propto t^\eta f(\Delta t^{1/\nu_\parallel}) \tag{19}$$

and

$$\overline{R}^2(t)=\frac{1}{\overline{n}(t)}\int d^dx\, x^2\rho(x,t)\propto t^z g(\Delta t^{1/\nu_\parallel})\ . \tag{20}$$

Notice that in simulations $\overline{n}(t)$ is averaged over the surviving samples only. From Eqs. (18), (19), and (20) one immediately sees that if $\phi(y)$, $f(y)$, and $g(y)$ are nonsingular at $y=0$, the asymptotic behavior of $P(t)$, $\overline{n}(t)$, and $\overline{R}^2(t)$ as $t\to\infty$ at p_c determines the critical exponents δ, η, and z:

$$P(t)\propto t^{-\delta}\ , \tag{21}$$

$$\overline{n}(t)\propto t^{\eta}\ , \tag{22}$$

$$\overline{R}^2(t)\propto t^{z}\ . \tag{23}$$

Away from the critical point, the behavior departs from a power law. In plots of $\ln P(t)$, $\ln\overline{n}(t)$, and $\ln\overline{R}^2(t)$ versus $\ln t$ we should see asymptotically a straight line at $p=p_c$. The curves for $P(t)$ and $\overline{n}(t)$ often have distinct positive (negative) curvature in the supercritical (subcritical) regime. This permits one to obtain a precise estimate for p_c. The asymptotic slopes of the curves at the critical point define the dynamic critical exponents δ, η, and z. The power-law behavior at criticality is often modified by corrections to scaling, so that, e.g., $P(t)$ is more accurately given by

$$P(t)\propto t^{-\delta}(1+at^{-1}+bt^{-\delta'}+\cdots)\ . \tag{24}$$

Similar expressions are expected to hold for $\overline{n}(t)$ and $\overline{R}^2(t)$. In order to estimate the critical exponents it is very useful to look at the local slopes:

$$-\delta(t)=\frac{\ln[P(t)/P(t/m)]}{\ln(m)}\ , \tag{25}$$

and similarly for $\eta(t)$ and $z(t)$. In the present work $m=5$. In plots of the local slopes versus $1/t$ one sees that the curves for the off-critical p values veer up or down, corresponding to p lying in the supercritical or subcritical regime, respectively. The critical exponents can be determined from the intercept of the critical curve with the y axis.

2. Simulation results

In the simulations of the PCP presented here we always started, at $t=0$, with a single pair at the origin. The surrounding configurations were chosen in different ways in order to check the sensitivity to the initial configuration. In one set of simulations the lattice was empty, in other simulations the sites were occupied at random (according to various algorithms) but so that no other pairs were present, and in the final set of simulations we let the dynamics of the PCP itself generate an absorbing state which we then used as the basis for the initial configuration. As the number of pairs is very small, the efficiency of the algorithm is greatly improved by keeping a list of all pairs. In each step a pair is chosen at random and removed with probability p. Otherwise, a nearest neighbor is chosen randomly and a new particle is placed there, provided the site is empty. After each attempted change time is incremented by $1/n(t)$, where $n(t)$ is the number of pairs prior to the update. Thus one time step equals on the average one attempted update per lattice site. For each value of p investigated, a number N_S of independent samples were simulated up to a maximal duration of t_M time steps, though most runs stopped earlier because all pairs had disappeared. In this study we used $N_S=(1-2)\times10^5$ and $t_M=2000$.

Empty initial configuration. In this set of simulations we start from an initial configuration consisting of an empty lattice, with the exception of a particle-pair at the center of the lattice. This state is certainly not close to a

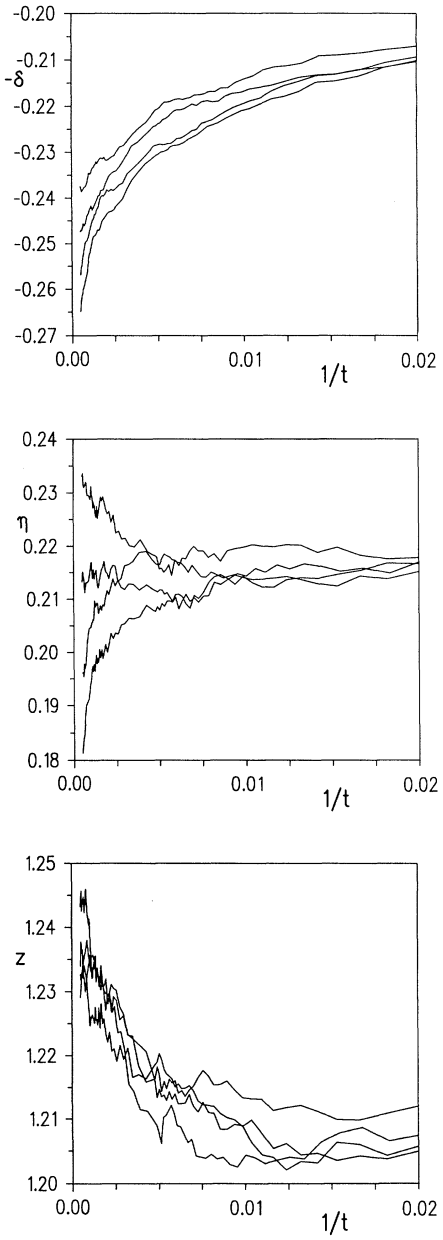

FIG. 10. Local slopes $-\delta(t)$ (left panel), $\eta(t)$ (middle panel), and $z(t)$ (right panel) as obtained from the simulation results when starting from an empty lattice except for a single pair at the central sites. Each panel contains four curves with, from top to bottom, $p=0.0770$, 0.0771, 0.0772, and 0.0773.

"typical" absorbing state of the PCP, but we study it here in order to see just how sensitive the critical parameters are to the initial configuration. In Fig. 10 we show the local slopes $-\delta(t)$, $\eta(t)$, and $z(t)$ versus $1/t$ for various values of p in the vicinity of the critical point. As can be seen, this initial configuration actually predicts the correct value for p_c. The estimates for the critical exponents $\delta=0.250(5)$, $\eta=0.215(5)$, and $z=1.238(4)$ are, however, not at all in agreement with those of directed percolation $\delta=0.160(1)$, $\eta=0.314(3)$, and $z=1.266(7)$ [17,22,46]. Note also that the critical exponents violate the scaling relation [17] $4\delta+2\eta=dz$, where d is the spatial dimension of the lattice.

Random initial configurations. As we have just seen, the "empty" initial configuration does not predict DP critical exponents, and it is therefore of interest to explore other choices of the initial configuration. In this section we study two random initial configurations which might be closer to a typical absorbing state for the PCP. In the first such configuration there are no correlations except for nearest-neighbor exclusion. We generate this configuration by occupying site i with probability $\frac{1}{2}$, provided site $i-1$ is not occupied already. Figure 11 shows the local slopes as obtained from this uncorrelated configuration. This choice of initial configuration again yields a p_c value, in agreement with the time-independent studies. This time the estimates for the critical exponents $\delta=0.130(5)$, $\eta=0.335(10)$, and $z=1.26(1)$ are closer to the DP values, though definitely not in agreement with them. The critical exponents again violate $4\delta+2\eta=dz$, although the discrepancy is smaller than in the case of the exponents obtained from the "empty" initial configuration.

The other random initial configuration is generated via random sequential adsorption (RSA) with nearest-neighbor exclusion. In RSA one starts from an empty lattice. The dynamics is very simple, as we simply choose a site at random and occupy it with a particle given that all nearest neighbors are empty, i.e., every adsorbed particle excludes its nearest neighbors from being possible adsorption sites. This procedure is continued until all sites are either occupied or excluded by a nearest-neighbor particle, i.e., we stop when there are no remaining triplets of empty sites. Figure 12 shows the local slopes as obtained from the RSA-type initial configuration. We see once again that the initial configuration predicts the correct value for p_c. This time the estimates for the critical exponents $\delta=0.0955(5)$, $\eta=0.38(1)$, and $z=1.28(1)$ depart even further from the DP values. Again the critical exponents do not satisfy the scaling relation $4\delta+2\eta=dz$.

System-generated initial configuration. In the final set of simulations we use the dynamics of the PCP to generate the initial configuration. We do this by starting with a small lattice of length L_I completely covered with particles. Then we let the dynamics of the PCP evolve at the p value under investigation until an absorbing state is reached. We now duplicate this absorbing state a number of times until the lattice used in the time-dependent simulations is covered. The initial configuration thus consists of a number of copies placed next to each other of an absorbing state obtained from a fairly small lattice. Remember that the lattice used in the time-dependent simulations is quite large in order to ensure that no particles ever reach the borders. Once this initial configuration has been generated, we place a particle pair at the center of the lattice, while vacating the neighbors if they happen to be occupied, so that we once again start from a configuration with just a single particle pair. In

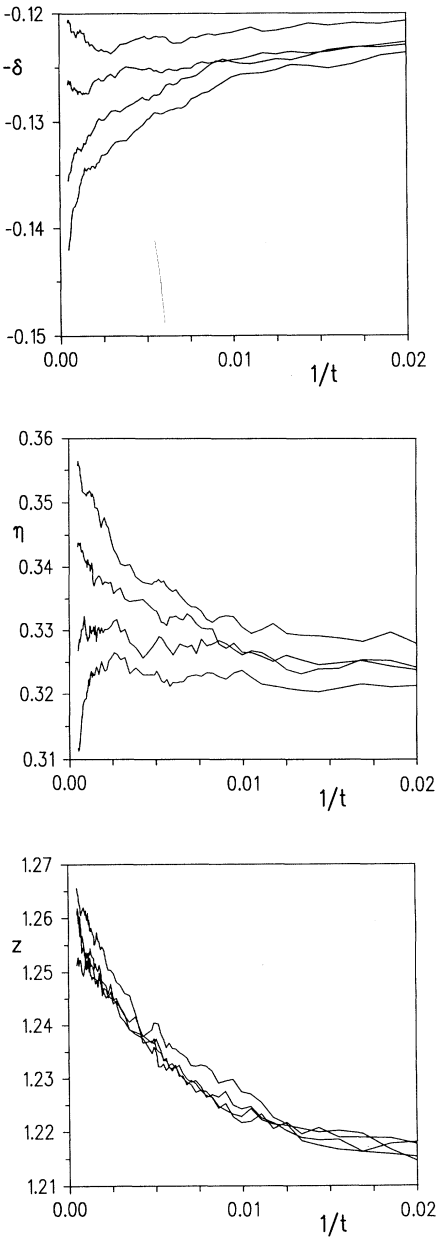

FIG. 11. Local slopes $-\delta(t)$ (left panel), $\eta(t)$ (middle panel), and $z(t)$ (right panel) as obtained from the simulation results when starting from a configuration where each site is occupied with probability $\frac{1}{2}$ but so that no pairs are present except for a single pair at the central sites. Each panel contains four curves with, from top to bottom, $p=0.0770$, 0.0771, 0.0772, and 0.0773.

Fig. 13 we show the local slopes as obtained by this procedure with $L_I=500$. The results were obtained by averaging over 100 different initial configurations and 1000 independent samples for each such configuration. As usual, we see that the initial configuration predicts p_c correctly. This time the estimates for the critical exponents $\delta=0.160(3)$, $\eta=0.310(5)$, and $z=1.260(5)$ agree fully with the exponents for directed percolaton. We have thus finally found a way to generate an appropriate initial configuration.

3. *Discussion*

Above we have studied several ways of choosing an initial configuration to be used in time-dependent simulations. The simulation results clearly show that the "best" (if not only) way of choosing the initial configuration is to use the system's own dynamics to generate the basis for the initial configuration. All the other ways we tried led to critical exponents which differ significantly from the expected DP values and which, moreover, violate hyper-

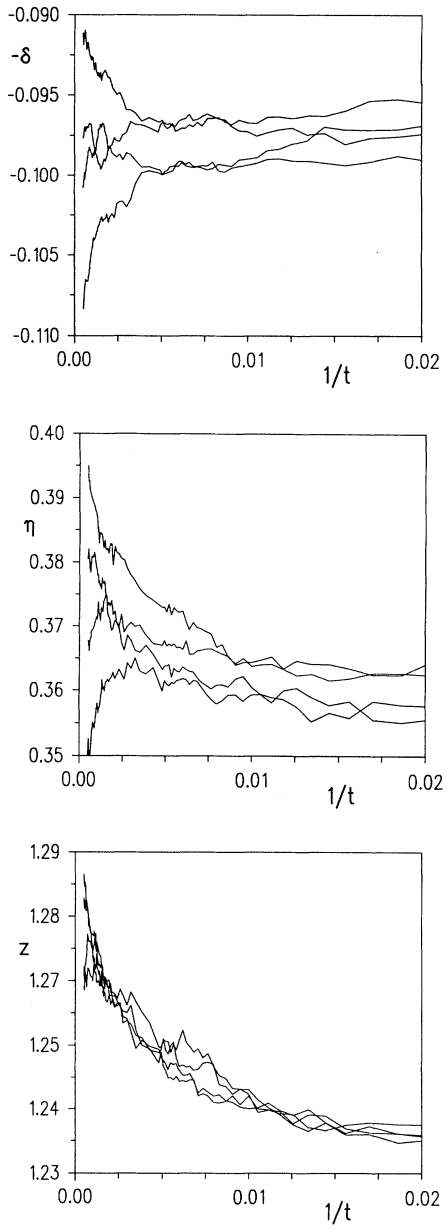

FIG. 12. Local slopes $-\delta(t)$ (left panel), $\eta(t)$ (middle panel), and $z(t)$ (right panel) as obtained from the simulation results when starting from a configuration generated from random sequential adsorption with nearest-neighbor exclusion. Each panel contains four curves with, from top to bottom, $p=0.0770$, 0.0771, 0.0772, and 0.0773.

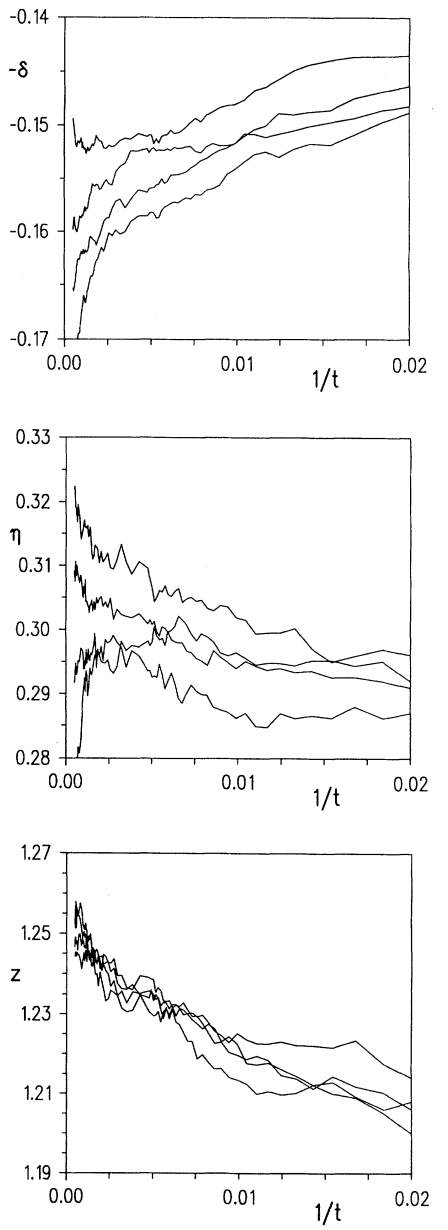

FIG. 13. Local slopes $-\delta(t)$ (left panel), $\eta(t)$ (middle panel), and $z(t)$ (right panel) as obtained from the simulation results when starting from a configuration generated from an absorbing state of a 500-site-long lattice. Each panel contains four curves with, from top to bottom, $p=0.0770$, 0.0771, 0.0772, and 0.0773.

scaling. The results do, however, contain two rather surprising features. First of all, the measured quantities still follow power laws, and secondly, p_c is predicted correctly irrespective of the initial configuration. The only indication that something might be "wrong" thus comes from the failure of the predicted exponent values to obey the hyperscaling relation.

The "empty" initial configuration does not contain any particles and is thus very untypical, and the production of new pairs is suppressed. The chance of a pair having a next-nearest-neighbor particle is very small, and each new particle is unlikely to produce more than one additional pair (a pair turning into a triplet increases the number of pairs by one). In a more realistic absorbing state it would be quite likely that a pair had a next-nearest-neighbor particle, and the eventual creation of a new particle would thus be likely to produce *two* additional pairs. We believe this is reflected in the values for the exponent, i.e., η is smaller and δ is greater than the DP values, showing that pairs are produced too slowly and samples die out too quickly. The two random initial configurations seem to lead to an overproduction of pairs (η is larger than the DP value), probably because the average concentration of particles is too large, and thus likewise for the probability of finding a next-nearest-neighbor particle to a given pair. This is certainly the case with the RSA initial configuration, as there can never be more than two empty sites next to one another, which clearly is a feature unrealistic of a "typical" absorbing state for the PCP.

An objection that can be raised to the arguments given above is that one normally assumes that a system at criticality should build up the correct correlations on its own. In steady-state simulations one normally does not worry about the initial configuration; e.g., in the simulations of the PCP we could have started, say, from a random initial configuration with some preset concentration of pairs. We would not expect this to influence the steady-state behavior. There is, however, a major difference between steady-state and time-dependent simulations in that in steady-state simulations we would always start from a homogenous initial configuration, and as the system evolves it will build up correlations and eventually "forget" the initial configuration. In time-dependent simulations we start from a highly inhomogeneous configuration, as the locus of activity is restricted initially to the origin. As a sample evolves from this state, the activity of a surviving sample will spread out, and inside this activity zone one might expect that the correct correlations should build up. However, as the activity zone spreads it will always meet the environment of the initial configuration and there is thus no way in which the sample can erase the memory of the initial state. The local environment for a growing cluster of pairs and leftover particles in the "empty" configuration will always be void of particles.

IV. THE DIMER REACTION MODEL

A. Study of poisoning times

A preliminary series of steady-state simulations indicated that the critical point is near 0.2640. But since small uncertainties in p_c can lead to substantial errors in exponent estimates, we require a more precise value. A reliable method for determining p_c in models of this kind is finite-size scaling analysis of the mean poisoning time [31]. Starting with an empty lattice of L sites (with periodic boundary conditions), we allow the process to evolve until it becomes trapped in an absorbing configuration. A set of M such evolutions are simulated and the time $\tau(p,L)$ for exactly half the set to poison is recorded. This procedure is repeated N times, and the mean and standard deviation of the mean determined, yielding our best estimate for $\tau(p,L)$ and the statistical uncertainty of the estimate. We studied lattices of size $L=20-1000$, with N decreasing from 2000 for $L=20-50$ for $L=1000$; $M=100$ throughout.

As discussed in Sec. III B 2, finite-size scaling theory implies that at the critical point the lifetime has a power-law dependence on system size, $\tau(p_c,L)\propto L^{\nu_\parallel/\nu_\perp}$. For $p<p_c$ τ increases exponentially with L, while for $p>p_c$ the growth is slower than a power law. Thus we can determine the location of the critical point and also compare the exponent ratio with its expected value. To search for power-law behavior and at the same time deviations from this exponent ratio, we plot $\ln\tau-(\nu_\parallel/\nu_\perp)\ln L$ versus $\ln L$, with $\nu_\parallel/\nu_\perp=1.579$. Off-critical reaction rates show up as curved graphs in such a plot; a nonzero slope of the linear (critical) graph signals an exponent ratio different from that of DP. From the data shown in Fig. 14 it is clear that $p_c=0.264\,00(5)$ (the graphs for 0.2639 and 0.2641 have noticeable curvature), and that there is no significant deviation from the DP exponent ratio. This is our first indication that the DR belongs to the directed percolation class.

B. Steady-state simulations

We performed extensive steady-state simulations of the DR on periodic lattices of size 1000, 2000,

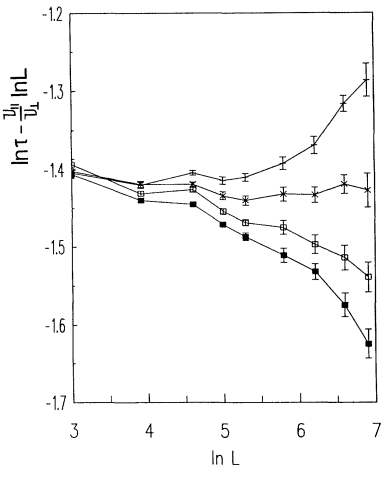

FIG. 14. $\ln\tau-\nu_\parallel/\nu_\perp$ vs $\ln L$. τ is the mean poisoning time, starting from an empty lattice. Directed percolation values are used for the exponents. +, $p=0.2639$; ×, $p=0.2640$; □, $p=0.2641$; ■, $p=0.2642$.

4000, . . . , 32 000. We monitored ρ_o and ρ_p, discarding results from the initial portion of any study which showed transient behavior. Density estimates were derived from a set of between 5 and 24 runs. Close to the critical point successive runs may not be independent, and so we used the block averaging procedure of Flyvbjerg and Petersen in estimating uncertainties [53]. Estimates at a given p were obtained for a series of lattice sizes until no significant change was observed upon doubling L. The only exception to this rule is our last data point, at $p=0.2635$ (quite near p_c), for which the $L=16\,000$ and 32 000 studies yielded $\rho_o=0.106(3)$ and 0.112(2), respectively. Near the critical point we used very long runs, extending to about 2×10^6 lattice updates for the largest system size, and considerably more for smaller lattices. We studied two or more (in most cases, eight) independent realizations for the process to derive our estimates.

The results of the steady-state simulations are shown in Fig. 15. The order parameter exponent β is defined via the expression $\rho_o \propto (p_c-p)^{\beta}$, where ρ_o is the density of open sites. Similarly, we may define β' through $\rho_{p,c}-\rho_p \propto (p_c-p)^{\beta'}$, where $\rho_{p,c}$ is the particle density at the critical point. Analysis of the data involves two adjustable parameters p_c and $\rho_{p,c}$, which are, however, tightly constrained by estimates obtained independently of the steady-state simulations. Within the limits imposed by these estimates, we find the best linear fit on log-log plots of ρ_o and $\rho_{p,c}-\rho_p$ using $p_c=0.263\,95$ and $\rho_{p,c}=0.419$. These are shown in Fig. 16. Straight-line best fits to the 15 points nearest p_c yield $\beta\simeq0.286$ and $\beta'\simeq0.297$. Since we expect $\beta=\beta'$ on general grounds (there is no reason to suspect *two* critical fields [25]), we estimate $\beta=0.290(15)$, which is consistent with the DP value $\beta=0.2769(2)$ [46].

C. Nature of the poisoned states

Given the vast number of possible absorbing configurations (AC's), it is of interest to examine the properties of the AC's generated by the DR near the critical point. Such information is also required as a prelude to time-dependent simulations. We have seen that in an AC occupied sites alternate with one- or two-site gaps. In other words, an AC is characterized by N, the number of particles, and a sequence $g_1, \ldots, g_N$ of binary random variables ($g_i=1$ and 2, being the length of gap i). At the minimum, we need to know the probability $p(1)=\text{Prob}[g=1]$ and the pair correlation $C(n)=\langle g_i g_{i+n}\rangle-\langle g_i\rangle^2$. A set of 300 AC's generated on an (initially empty) lattice of 1000 sites at p_c yielded $p(1)=0.625(3)$, $C(1)=0.048(2)$, and $C(i)\approx0$ for $i\geq2$. Thus AC's generated by the critical DR are statistically well characterized by the one-site probabilities and the nearest-neighbor correlation, or equivalently by the transition probabilities $p(i|j)$ $(i,j=1,2)$.

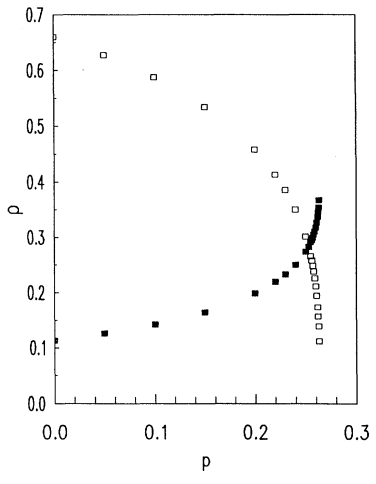

FIG. 15. Steady-state densities of open sites (□) and particles (■) vs p. Error bars are smaller than the size of the symbols.

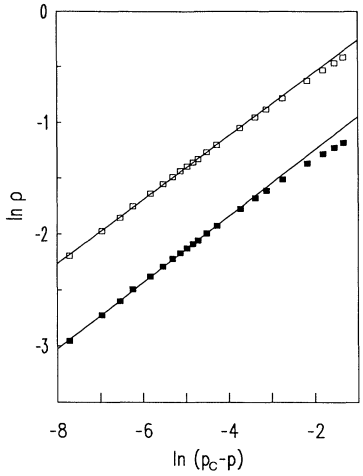

FIG. 16. $\ln\rho_o$(□) and $\ln(\rho_{p,c}-\rho_p)$ (■) vs $\ln(p_c-p)$ for the steady-state DR. The straight lines have slopes 0.286 (upper) and 0.297 (lower).

D. Time-dependent scaling behavior

In time-dependent simulations one studies the evolution of the system, starting from a nearly absorbing configuration, in this case one with a single open site. For the DR and PCP there are of course many possible near-absorbing configurations, and we shall investigate several different kinds. To begin, we consider initial states whose statistics match those of critical system-generated AC's. Sites 0, +1, and −1 are initially vacant, while sites $2, \ldots, L$ form an absorbing sequence *OGOGO* . . . , where the first gap (i.e., site 3) is given length 1 and all subsequent gaps are generated randomly using the transition probabilities found in actual critical AC's. The absorbing sequence for sites $-2, \ldots, -L$ is generated in the same manner. Thus the initial configuration is statistically indistinguishable from a critical system-generated AC, with one open site inserted. We performed 40 000 realizations of the evolution at $p=0.2640$, each starting from a different randomly generated initial configuration, and followed the survival probability $P(t)$, the mean number of open sites $\bar{n}(t)$, and

TABLE I. Exponents for time-dependent behavior of the critical DR with various kinds of initial states, characterized by particle density $\rho_{p,i}$ and nearest-neighbor correlation $C(1)$.

Exponents		Directed percolation δ	η	z	$z-4\delta-2\eta$
		0.160(2)	0.314(3)	1.264(10)	0.006(24)
		Dimer reaction model			
$\rho_{p,i}$	$C(1)$	δ	η	z	$z-4\delta-2\eta$
0.418	0.048	0.160(2)	0.304(4)	1.252(6)	0.008(22)
0.418	0	0.154(3)	0.305(3)	1.256(6)	0.030(22)
0.418	0.738	0.158(2)	0.298(4)	1.244(6)	0.016(20)
0.418	−0.563	0.160(2)	0.300(4)	1.256(6)	0.016(22)
0.5	0	0.205(5)	0.250(5)	1.240(6)	−0.08(4)
0.38	0	0.133(2)	0.327(3)	1.258(10)	0.072(24)
$\frac{1}{3}$	0	0.107(2)	0.362(3)	1.267(6)	0.115(20)

the mean-square spread $R^2(t)$ of open sites from the origin. Clear evidence of power-law behavior is observed, with the exponents δ, η, and z (obtained through analysis of local slopes), close to the DP values (see Fig. 17 and Table I). The off-critical reaction rates $p=0.2639$ and 0.2641 yield slight deviations from power-law behavior.

How are the exponents affected when we change the correlation between neighboring gaps in the initial configuration? We are unable to detect any significant dependence upon the nearest-neighbor gap correlation when we compare the "natural" (weakly correlated) case with (1) $C(1)=0$, i.e., independent Bernoulli trials for the gap lengths, (2) a high correlation, $C(1)=0.738$, or (3), negative correlation, $C(1)=-0.5625$. In summary, starting from an initial configuration whose particle density matches that of a critical AC, the evolution of the critical DR exhibits the same kind of power-law behavior as directed percolation.

Next we investigate the effect of varying the particle concentration in the initial configuration. For the maximally occupied initial state (. . . *oxoxoooxoxo* . . .), the evolution at p_c again shows power-law behavior, but with very different exponents: $\delta\approx0.20$, $\eta\approx0.26$, and $z\approx1.246$. Starting near the minimally occupied AC, the exponents are again non-DP, but are skewed in the opposite direction. These power laws are shown in Fig. 17. Random initial configurations with particle density 0.38, closer to but still less than the "natural" value of 0.418(1),

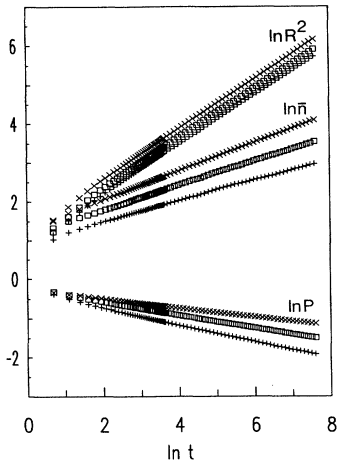

FIG. 17. $\ln P(t)$, $\ln\bar{n}(t)$, and $\ln R^2(t)$ vs $\ln t$ for the critical DR starting from various initial configurations. □, $\rho_{p,i}=0.418$; +, $\rho_{p,i}=\frac{1}{2}$; ×, $\rho_{p,i}=\frac{1}{3}$.

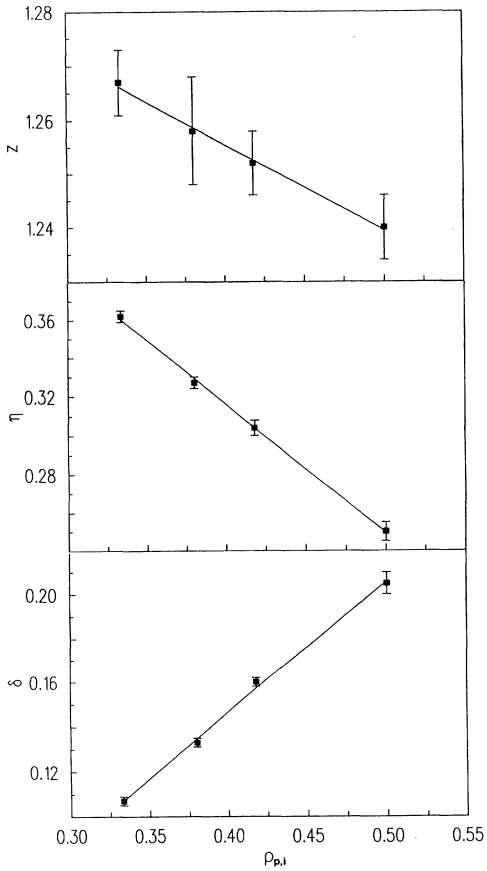

FIG. 18. Variation of the exponents δ, η, and z with the initial particle density in the critical DR. Straight lines are least-squares linear fits to the data.

yield similar but smaller deviations in the exponent values. That δ increases while η and z decrease with increasing initial particle density $\rho_{p,i}$ is consistent with the notion that it is more difficult for open sites to invade a denser system. It appears that the exponent values vary *continuously* with the initial particle density. The variation of z with ρ_p is rather small, but still significant.

Our findings on the exponents for time-dependent behavior are summarized in Table I. We observe that the η and z values for the DR (starting with $\rho_p = 0.418$) are slightly below the DP values, which may reflect that p_c is slightly below 0.2640 (the steady-state results also suggest this possibility). In any case the present data provide no reason to doubt that the DR belongs to the directed percolation class. We also note that the hyperscaling relation $dz = 4\delta + 2\eta$ is violated by the DR starting from initial configurations with ρ_p different from 0.418. Figure 18 shows that the exponents have an approximately linear dependence upon initial particle density.

V. SUMMARY

Previous studies of critical phenomena at a transition into a nonunique absorbing state [39–41] led us to expect nondirected percolation behavior in the pair contact process and the dimer reaction model. Thus the very clear evidence of DP exponents for these models comes as a surprise. On the other hand, the pair contact process and the dimer reaction model may be described by a scalar order parameter, such as the concentration of pairs in the PCP, which vanishes identically in the absorbing states. Our results thus provide further support of the idea [42] that the DP conjecture can be extended to models with infinitely many absorbing states, at least as long as the absorbing states can be uniquely characterized by the vanishing of a single quantity.

While the static critical behavior falls in the DP class, the time-dependent behavior does so only if we are careful to provide an initial near-absorbing configuration which matches the particle density in a critical, system-generated absorbing configuration. Other initial densities yield a family of *nonuniversal, critical growth processes.* They are "critical" in that they exhibit power-law behavior. But the exponents vary continuously with the initial density, and violate the hyperscaling relation implied by the basic scaling hypothesis [17]. These growth processes are well defined, but only the ones with the "critical" initial density appear to have a corresponding stationary counterpart.

The one-dimensional versions of the PCP and DR, models with rather different evolution rules, both fall in the DP universality class. In light of this, further studies of these models in higher dimensions, and of the models proposed by Albano and Köhler and ben-Avraham, would be of great interest. Note that the absorbing states in the dimer-dimer and dimer-trimer models are uniquely characterized by the vanishing of the density of nearest-neighbor empty sites. Though the exponent estimates are only marginally consistent with directed percolation, it does not seem impossible that these models also belong to the DP universality class. The non-DP behavior of the model proposed by Grassberger, Krause, and von der Twer [39], and of BAW's with an even number of offspring [37], may be due to the additional conservation law (particle number conserved modulo 2) not present in other models.

ACKNOWLEDGMENTS

One of us (I.J.) gratefully acknowledges the support of the Danish Research Academy. The simulations were performed on the facilities of the University Computing Center of the City University of New York.

*Electronic address: INJLC@CUNYVM.BITNET
†Electronic addres: DICKMAN@LCVAX.BITNET

[1] G. Nicolis and I. Prigogine, *Self-Organization in Non-equilibrium Systems* (Wiley-Interscience, New York, 1977).
[2] H. Haken, *Synergetics* (Springer-Verlag, New York, 1983).
[3] T. E. Harris, Ann. Prob. **2**, 969 (1974).
[4] T. M. Liggett, *Interacting Particle Systems* (Springer-Verlag, New York, 1985).
[5] R. Durrett, *Lecture Notes on Particle Systems and Percolation* (Wadsworth, Pacific Grove, CA, 1988).
[6] F. Schlögl, Z. Phys. B **253**, 147 (1972).
[7] H. K. Janssen, Z. Phys. B **42**, 151 (1981).
[8] P. Grassberger, Z. Phys. B **47**, 365 (1982).
[9] S. Wolfram, Rev. Mod. Phys. **55**, 601 (1983).
[10] W. Kinzel, Z. Phys. B **58**, 229 (1985).
[11] P. Rujàn, J. Stat. Phys. **49**, 139 (1987).
[12] Several articles about directed percolation may be found in *Percolation Structures and Processes,* edited by G. Deutsher, R. Zallen, and J. Adler, Annals of the Israel Physical Society Vol. 5 (Hilger, Bristol, 1983).
[13] J. L. Cardy and R. L. Sugar, J. Phys. A **13**, L423 (1980).
[14] H. K. Janssen, Z. Phys. B **58**, 311 (1985).
[15] P. Grassberger, J. Phys. A **22**, 3673 (1989).
[16] P. Grassberger and K. Sundemeyer, Phys. Lett. **77B**, 220 (1978).
[17] P. Grassberger and A. de la Torre, Ann. Phys. (N.Y.) **122**, 373 (1979).
[18] V. N. Gribov, Zh. Eksp. Teor. Fiz. **53**, 654 (1967) [Sov. Phys. JETP **26**, 414 (1968)].
[19] V. N. Gribov and A. A. Migdal, Zh. Eksp. Teor. Fiz. **55**, 1498 (1968) [Sov. Phys. JETP **28**, 784 (1969)].
[20] H. D. I. Abarbanel, J. B. Bronzan, R. L. Sugar, and A. R. White, Phys. Rep. **21**, 119 (1975).
[21] M. Moshe, Phys. Rep. C **37**, 255 (1978).
[22] R. C. Brower, M. A. Furman, and M. Moshe, Phys. Lett. **76B**, 213 (1978).
[23] R. M. Ziff, E. Gulari, and Y. Barshad, Phys. Rev. Lett. **56**, 2553 (1986).
[24] P. Meakin and D. J. Scalapino, J. Chem. Phys. **87**, 731 (1987).
[25] G. Grinstein, Z.-W. Lai, and D. A. Browne, Phys. Rev. A **40**, 4820 (1989).
[26] I. Jensen, H. C. Fogedby, and R. Dickman, Phys. Rev. A

41, 3411 (1990).
[27] R. Dickman and M. Burschka, Phys. Lett. A **127**, 132 (1988).
[28] R. Dickman, J. Stat. Phys. **55**, 997 (1989).
[29] R. Dickman, Phys. Rev. B **40**, 7005 (1989).
[30] D. A. Browne and P. Kleban, Phys. Rev. A **40**, 1615 (1989).
[31] T. Aukrust, D. A. Browne, and I. Webman, Europhys. Lett. **10**, 249 (1989); Phys. Rev. A **41**, 5294 (1990).
[32] R. Dickman, Phys. Rev. A **42**, 6985 (1990).
[33] R. Bidaux, N. Boccara, and H. Chaté, Phys. Rev. A **39**, 3094 (1989).
[34] I. Jensen, Phys. Rev. A **43**, 3187 (1991).
[35] R. Dickman and Tania Tomé, Phys. Rev. A **44**, 4833 (1991).
[36] M. Bramson and L. Gray, Z. Warsch. Gebiete **68**, 3060 (1985).
[37] H. Takayasu and A. Yu. Tretyakov, Phys. Rev. Lett. **68**, 3060 (1992).
[38] I. Jensen, Phys. Rev. E **47**, 1 (1993).
[39] P. Grassberger, F. Krause, and T. von der Twer, J. Phys. A **17**, L105 (1983); P. Grassberger, J. Phys. A **22**, L1103 (1989).
[40] J. Köhler and D. ben-Avraham, J. Phys. A **24**, L621 (1991); D. ben-Avraham and J. Köhler, J. Stat. Phys. **65**, 839 (1992).
[41] E. V. Albano, J. Phys. A **25**, 2557 (1992); A. Maltz and E. V. Albano, Surf. Sci. **277**, 414 (1992).
[42] I. Jensen, Phys. Rev. Lett. **70**, 1465 (1993).
[43] P. J. Flory, J. Am. Chem. Soc. **61**, 1518 (1939).
[44] B. Widom, J. Chem. Phys. **44**, 3888 (1966); **58**, 4043 (1973).
[45] B. Widom, J. Chem. Phys. **43**, 3898 (1965).
[46] R. Dickman and I. Jensen, Phys. Rev. Lett. **67**, 2391 (1991); I. Jensen and R. Dickman, J. Stat. Phys. **71**, 89 (1993).
[47] J. W. Essam, K. De'Bell, J. Adler, and F. M. Bhatti, Phys. Rev. B **33**, 1982 (1986); J. W. Essam, A. J. Guttmann, and K. De'Bell, J. Phys. A **21**, 3815 (1988).
[48] Our notation for the critical exponents differs from that of directed percolation. β, $\nu_{\parallel}$, and $\nu_{\perp}$ are the same, but $\gamma^{\mathrm{DP}}=\gamma+\nu_{\parallel}+(1-d)\nu_{\perp}$. We used the latter relation to obtain the estimate for γ.
[49] M. E. Fisher, in *Critical Phenomena,* Proceedings of the International School of Physics "Enrico Fermi," Course XX, Varenna, Italy, 1971, edited by M. S. Green (Academic, New York, 1971); M. E. Fisher and M. N. Barber, Phys. Rev. Lett. **28**, 1516 (1972).
[50] M. N. Barber, in *Phase Transitions and Critical Phenomena,* edited by C. Domb and J. L. Lebowitz (Academic, New York, 1983), Vol. 8.
[51] A. Milchev, K. Binder, and D. W. Heermann, Z. Phys. B **63**, 521 (1986).
[52] For second-order equilibrium phase transitions this exponent is traditionally called z. For the type of nonequilibrium phase transitions studied here we will reserve z for another exponent that will be defined in the next section.
[53] H. Flyvbjerg and H. G. Petersen, J. Chem. Phys. **91**, 461 (1989).